Analyst

ROYAL SOCIETY OF CHEMISTRY

PAPER

View Article Online
View Journal | View Issue

Cite this: *Analyst*, 2025, **150**, 2270

Magnetic mesoporous carbon nanocomposites derived from bimetallic metal–organic frameworks for enrichment of low-abundance peptides†

Jia-Yuan Li,[a,b] Sen Zhang,[a] Wan-Yue Zhuang,[a] Feng Zhang,[a] Wei-Juan Zheng,[c] Li Mao[d] and Hong-Zhen Lian *[a]

Mesopore-structured cobalt and nickel metal–organic frameworks (Co/Ni-ZIF) were synthesized by a self-assembly method using Co and Ni as bimetallic centers and 2-methylimidazole as the organic ligand at room temperature. The resulting rhombic dodecahedral nanocomposites possessing rich mesopores with an average diameter of 4 nm were collected centrifugally and then carbonized under a nitrogen atmosphere to generate bimetallic magnetic porous carbon nanocomposites (Co/Ni-MCNs). After thorough characterization, the as-prepared Co/Ni-MCNs decorated with a graphite shell layer with pyridinic nitrogen were utilized in magnetic separation and enrichment of low-abundance peptides through hydrophobic and π–π stacking interactions. This is the first attempt to prepare mesoporous carbon materials having plentiful holes with bimetal MOFs as precursors, in which partial nickel-containing components served as sacrificial templates. Owing to the ordered structure, abundant mesopores, rich interaction sites, excellent magnetic properties and good compatibility with biological tissues, this proposed magnetic affinity probe has been successfully used in the identification of endogenous peptides in human urine and serum in combination with matrix-assisted laser desorption/ionization time of flight mass spectrometry (MALDI-TOF MS).

Received 4th February 2025,
Accepted 12th April 2025

DOI: 10.1039/d5an00127g

rsc.li/analyst

Introduction

Endogenous peptides play essential roles in regulating many physiological and pathological processes, such as growth factors, hormones and cytokines and so on.[1,2] It is well known that peptide mapping by matrix-assisted laser desorption/ionization time of flight mass spectrometry (MALDI-TOF MS) along with database searching is a major tool in current proteomics/peptidomics analysis because of its excellent mass accuracy, operational simplicity, and high speed, resolution, throughput and sensitivity.[3,4] Yet, the analysis of endogenous peptides using MS is always a challenge, owing to their extremely low concentrations in practical biological samples of complex matrices. Therefore, it is important to selectively separate and enrich low-abundance peptides prior to MS analysis.

To date, numerous materials and approaches have been widely developed for the capture of low-abundance peptides, including mesoporous carbon,[5] metal–organic frameworks (MOFs),[6] zeolite nanocrystals,[7] carbon nanotubes,[8,9] graphene oxide,[10] mesoporous silica microspheres,[11] poly(methyl methacrylate) (PMMA)-modified nanoparticles,[12–14] *etc.* In addition, thanks to the simple and convenient isolation from complex biological matrices, various core–shell magnetic nanoparticles have been extensively exploited for magnetic solid-phase extraction (MSPE) of low-abundance peptides, such as magnetic MOFs,[15–17] magnetic graphene,[18,19] magnetic silica microspheres,[20,21] Fe_3O_4@SiO_2@FTA,[22] $CuFeMnO_4$ nanospheres,[23] magnetic carbon microspheres,[24] C_8 functionalized magnetic materials,[25–28] Fe_3O_4@SiO_2@PMMA,[29] Fe_3O_4@nSiO_2@C_{60},[30] MNPs-L-DOPA/PEI-SP,[31] Fe_3O_4@CS@Au-L-Cys,[32] and others. Among them, magnetic porous carbon materials, with a high specific surface area, a

[a]*State Key Laboratory of Analytical Chemistry for Life Science, School of Chemistry & Chemical Engineering and Center of Materials Analysis, Nanjing University, 163 Xianlin Avenue, Nanjing 210023, China. E-mail: hzlian@nju.edu.cn; Fax: +86-25-83325180; Tel: +86-25-83686075*
[b]*School of Environmental and Safety Engineering, Nanjing Polytechnic Institute, 188 Xinle Road, Nanjing 210048, China*
[c]*State Key Laboratory of Pharmaceutical Biotechnology, School of Life Sciences, Nanjing University, 163 Xianlin Avenue, Nanjing 210023, China*
[d]*Ministry of Education (MOE) Key Laboratory of Modern Toxicology, School of Public Health, Nanjing Medical University, 101 Longmian Road, Nanjing 211166, China*

†Electronic supplementary information (ESI) available: Materials and reagents. Apparatus for characterization. SEM images, TEM images, EDS spectra, elemental mapping, FT-IR spectra, and N_2 absorption–desorption curves of Co/Ni-ZIFs. XPS spectra of Co/Ni-MCNs. Performance of Co/Ni-MCNs and other affinity probes in standard peptide enrichment. The amino acid sequence of identified peptides from BSA tryptic digests. Sensitivity and recyclability of Co/Ni-MCNs for peptide enrichment from BSA tryptic digests. Application of Co/Ni-MCNs for enrichment of endogenous peptides in human serum. Detailed comparison of Co/Ni-MCNs with previously reported magnetic affinity probes for low-abundance peptides. See DOI: https://doi.org/10.1039/d5an00127g

narrow pore-size distribution, good chemical resistance and biological affinity to organics, have been considered as very promising adsorbents for low-abundance peptide analysis due to hydrophobic and π–π stacking interactions between compatible carbon shells and peptides. However, it is still worthwhile to explore different metal oxide/metal@carbon core–shell nanostructures, because the existing fabrication approach is basically multi-step and time-consuming. Therefore, a new and simple method for preparing magnetic core–shell porous carbon materials as affinity probes for enriching endogenous peptides is required uninterruptedly.

MOFs are a rapidly growing class of porous crystalline hybrid materials with the remarkable characteristics of well-defined channels, as well as cavities of regular size and shape that can be easily tuned on a nanometer scale.[33] As a significant subclass of MOFs, zeolitic imidazolate frameworks (ZIFs) are composed of transition-metal cations and imidazole-based ligands, interconnected through cross-linking to form a framework structure. Among them, ZIF-67 is a self-assembled structure in which Co^{2+} ions are coordinated with the organic compound 2-methylimidazole (2-MIM). ZIF-67 and its derivatives enable the creation of materials with well-defined pore structures and tunable chemical functionality and have been explored for various applications, such as adsorption, separation, electrochemistry, catalysis, degradation and CO_2 uptake.[34–37] Moreover, doping transition metals into host ZIF-67 could help to regulate the structural characteristics with uniform size, porosity, *etc.*, to improve their intrinsic activity or capacity.[34,37] For example, using Ni^{2+} ions as the dopant into ZIF-67, the prepared Ni@ZIF-67 shows enhanced uptake performance in selective CO_2 adsorption compared to ZIF-67.[38] Benefitting from the fascinating properties above, MOFs including ZIFs have been demonstrated as ideal candidates for use as templates or precursors to synthesize nanoporous carbons,[39] metallic nanoparticles,[40,41] porous carbon-metallic nanocomposites,[42] and so forth. Highly symmetric Co_3O_4 porous dodecahedra with enhanced lithium storage capability were synthesized through preparation of a Co-containing ZIF-67 template with a rhombic dodecahedral morphology and subsequent thermal annealing.[43] Nanoporous carbon particles with magnetic Co nanoparticles (Co/NPC particles) were prepared by carbonization of ZIF-67 crystals towards efficient water treatment.[44] As for heteroatom-doped carbon materials, nickel oxide/cobalt/carbon nitride (Ni/Co/CN) nanocomposites facilitating the light-driven photocatalytic degradation of methylparaben, a preservative used in cosmetics and personal care products, were fabricated by introducing NiO nanoparticles into the conventional treatment process of ZIF-67.[45] Such ZIF-67-derived nanoporous metal oxides and carbon materials have a high surface area and interconnected pores, which are advantageous for their improved performance in several applications. Interestingly, the porous carbon materials employing MOFs as sacrificial templates and carbon precursors have potential for separation and enrichment of low-abundance endogenous peptides before MS analysis.

In the present study, we have proposed a facile and cost-effective approach for the preparation of hybrid magnetic core–shell mesoporous carbon nanocomposites (MCNs) for highly efficient enrichment of endogenous peptides using bimetallic MOFs (Co/Ni-ZIF) as precursors prior to MALDI-TOF MS analysis. Firstly, mesoporous Co/Ni-ZIF crystals were synthesized *via in situ* self-assembly at ambient temperature. Then, magnetic MOF-derived mesoporous carbon was acquired through thermal treatment of Co/Ni-ZIF crystals under a nitrogen atmosphere. After thorough characterization, the prepared Co/Ni-MCNs were utilized as the MSPE adsorbent for the pretreatment of angiotensin II and bovine serum albumin (BSA) tryptic digests. Finally, the Co/Ni-MCN affinity probe was used to selectively enrich low-abundance endogenous peptides in real human urine and serum.

Experimental section

The materials, reagents, samples and apparatus used in this work are listed in detail in the ESI.†

Synthesis of Co/Ni-ZIF precursors

ZIF-67 was fabricated *via* a one-pot self-assembly reaction following the procedures reported previously with slight modifications.[43,46] As shown in Scheme 1, $Co(NO_3)_2{\cdot}6H_2O$ (145.5 mg) was dissolved in 5 mL of deionized water to form a solution used as the central ion source for synthesizing the precursors, and 2-MIM (3.248 g) was dissolved in 15 mL of deionized water. Then, these two solutions were mixed together and stirred for 30 s, and the resulting solution was aged at room temperature for 24 h. After all of the precipitates (purple in color) had settled at the flask bottom, the powders were isolated *via* centrifugation, washed with ethanol and dried for further treatment. The procedure was also applied in the preparation of bimetallic Co/Ni-ZIF, except that $Co(NO_3)_2{\cdot}6H_2O$ was replaced partially or totally with $Ni(NO_3)_2{\cdot}6H_2O$. In detail, different mass ratios of $Co(NO_3)_2{\cdot}6H_2O$ and $Ni(NO_3)_2{\cdot}6H_2O$ (5 : 0, 2 : 1, 1 : 1, 1 : 2 and 0 : 5, respectively) were dissolved in 5 mL of deionized water. After comparison, the Co/Ni mass ratio of 1 : 1 was finally chosen to obtain the bimetallic MOF, and the subsequent centrifugation treatment was conducted at a speed of 2000 rpm to isolate the rhombic dodecahedral MOF precursors, denoted as Co/Ni-ZIF unless stated otherwise, from the reactant mixture dispersed in ethanol.

Carbonization of the Co/Ni-ZIF precursor to form Co/Ni-MCNs

The preparation method for the magnetic mesoporous Co/Ni-MCNs is also illustrated in Scheme 1. Referring to the carbonization process of ZIF-67,[44] the rhombic dodecahedral Co/Ni-ZIF precursors were directly heated under a nitrogen flow at 600 °C. The temperature inside the furnace was gradually increased from room temperature to the target temperatures with a heating rate of 5 °C min^{-1}. After the temperature reached 600 °C, the resulting powders were annealed for 5 h and then cooled at room temperature. Lastly, the powders were

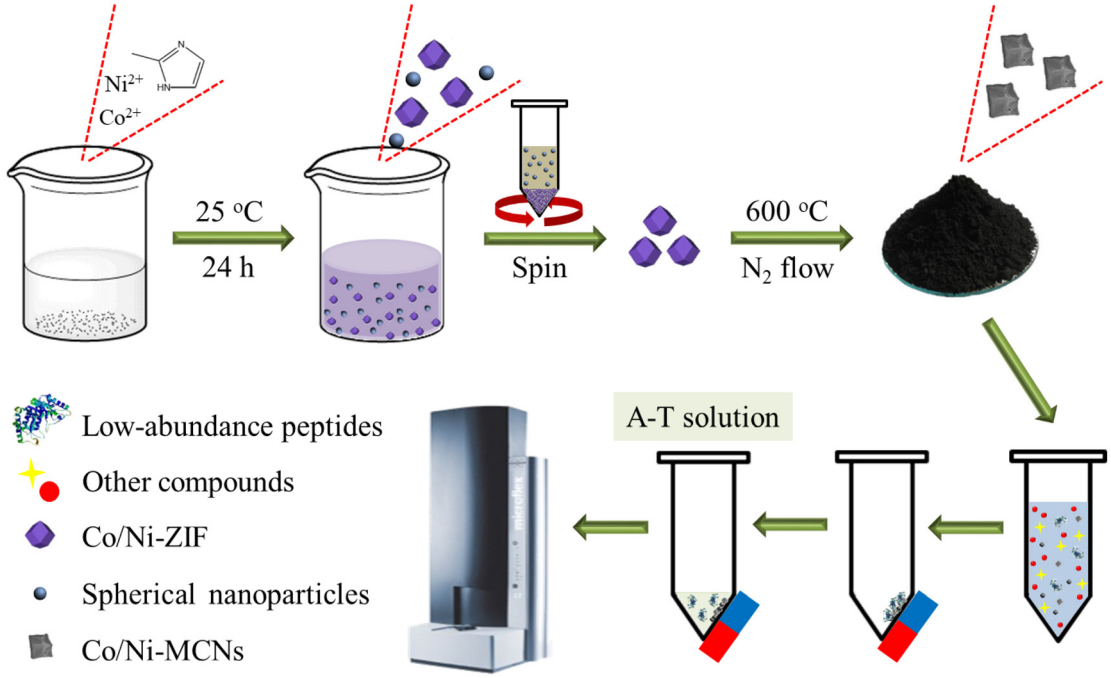

Scheme 1 Schematic illustration of the preparation strategy of Co/Ni-MCN nanocomposites and the procedure for enrichment of low-abundance peptides using the affinity probes.

gathered and their color was found to change from purple to black. These black products were denoted as Co/Ni-MCNs.

Tryptic digestion of proteins

BSA (1.0 mg) was dissolved in 1.0 mL of 50 mmol L^{-1} NH_4HCO_3 solution (pH 8.3) to form a substrate solution and then digested at 37 °C for 18 h with trypsin at a ratio of enzyme-to-substrate of 1 : 40 (wt/wt). An aliquot of the above proteolytic digests was frozen at −80 °C for standby application. The frozen digests were thawed and then diluted to the target concentration with water before use.

Enrichment of low-abundance peptides

A schematic representation of the workflow system for enrichment of low-abundance peptides by a Co/Ni-MCN adsorbent is shown in Scheme 1. In detail, 500 μL (10 nM) of BSA digests were mixed with 5 μL of 20 mg mL^{-1} Co/Ni-MCN suspension and vortexed for 15 min. Then, the affinity probes with trapped target peptides were isolated by using a magnet and washed with 500 μL of water three times. Afterwards, the enriched peptides were eluted with 5 μL of elution solution containing 60% acetonitrile (ACN) and 1.0% trifluoroacetic acid (TFA) (v/v, denoted as A–T solution), and the supernatant was magnetically collected for mass spectrometric (MS) analysis. For enriching peptides from human urine and serum, 500 μL of diluted sample were mixed with 5 μL of 20 mg mL^{-1} Co/Ni-MCN suspension and vortexed for 15 min. Then, the affinity probes with trapped target peptides were isolated by using a magnet and washed with 500 μL of water three times. Afterwards, the enriched peptides were eluted with 5 μL of A–T solution, and the supernatant was magnetically collected for MS analysis.

MALDI-TOF MS analysis

0.5 μL of eluate was deposited on a MALDI plate, and 0.5 μL of α-cyano-4-hydroxycinnamic acid (CHCA) (10 mg mL^{-1} in 50% ACN/water containing 1% H_3PO_4 solution, v/v) was introduced as a MALDI matrix to perform the MS analysis in positive ion mode using a 4800 Proteomics Analyzer (Applied Biosystems, Framingham, CT, USA) with an Nd-YAG laser at a wavelength of 355 nm, a repetition rate of 200 Hz, and an acceleration voltage of 20 kV. Mass spectra were obtained by accumulation of 3000–4000 consecutive laser shots.

Results and discussion

Characterization of Co/Ni-ZIF precursors

ZIF-67 and Co/Ni-ZIF precursors were one-pot synthesized respectively with different mass ratios of Co and Ni ions with over-stoichiometric 2-MIM at a fixed dose. As shown in the scanning electron microscopy (SEM) image (Fig. S1A†), the obtained ZIF-67 nanoparticles (the mass ratio of $Co(NO_3)_2$ to $Ni(NO_3)_2$ was 5 : 0) presented various polyhedral shapes of different sizes. Upon the addition of a nickel source ($Ni(NO_3)_2$), however, the surface of the material became a bit rough with the increase of the mean grain size to a mass ratio of 2 : 1 (Fig. S1B†). When the mass ratio of $Ni(NO_3)_2$ was equal to that of $Co(NO_3)_2$, the products had good uniformity with two regular morphologies (rhombic dodecahedral and spheri-

cal nanoparticles, respectively) (Fig. S1C†), which was confirmed by clearer SEM re-shots (Fig. S2A and S2B†) after centrifugal separation. It was further found that there were plentiful mesopores on the surface of rhombic dodecahedra, while no pores were on the surface of nanospheres (Fig. S3A and S3B†). In addition, the distributions and contents of Co and Ni elements in the MOFs were revealed by the corresponding elemental mapping (Fig. S3C and S3D†) and EDS results (Fig. S4†), indicating that they coexisted and were evenly dispersed in these two structures. Moreover, EDS results showed that the mass ratios of Co and Ni elements were different in the dodecahedral and spherical structures. The content of Co was much more than that of Ni in the rhombic dodecahedra, while the contents of the above two elements were almost equal in the spheres, although the dose mass of Co was equal to that of Ni during the synthesis process. This is because of the collapse of Ni-containing template fragments in ethanol, forming abundant pores on the surface of the dodecahedral structure. In contrast, the spherical nanoparticles without a porous structure contained as much Co element as Ni element, suggesting that the fraction of the spherical structure formed by Ni^{2+} was relatively stable in ethanol. The appearance of nanospheres resulted likely from the equal ratio of Co^{2+} and Ni^{2+} forming a Ni–Co binary hydroxide compound under the alkaline conditions of 2-MIM.[47,48] In brief, two kinds of nanoparticles possessed completely different morphography and elemental composition. When the dosage of Ni further increased, a lot of small particles attached to the surface of enlarged polyhedra were observed at a Co/Ni ratio of 1 : 2, making the surface of the polyhedra very rough (Fig. S1D†). Finally, when Co was completely replaced by Ni, no polyhedra and spheres were observed except for a yellow ointment (Fig. S1E†). This yellow product formed at a ratio of 0 : 5 could be dissolved in ethanol, supporting the speculation that the structure of the complex formed by Ni^{2+} and 2-MIM was unstable and collapsed in ethanol. The above phenomena illustrated that the introduction of Ni for the fabrication of Ni-doped ZIF-67 generated two different kinds of nanoparticles, and the dose ratio of Co and Ni sources had a significant impact on the structure and feature of the bimetallic MOF precursors. Thus, a Co^{2+}/Ni^{2+} mass ratio of 1 : 1 was chosen to obtain Co/Ni-ZIF containing two regular nanoparticles. Ultimately, the mesoporous rhombic dodecahedral nanoparticles as Co/Ni-ZIF precursors were isolated *via* centrifugation from the spherical nanoparticles for subsequent carbonization to prepare Co/Ni-MCNs.

The SEM and transmission electron microscopy (TEM) images of the selected Co/Ni-ZIF are shown in Fig. 1A and B, respectively. The corresponding positions and intensities of the FT-IR absorption peaks (Fig. S5†) of Co/Ni-ZIF were in agreement with those of ZIF-67,[49] because 2-MIM was a dominant ligand for these two MOFs. The structure of Co/Ni-ZIF

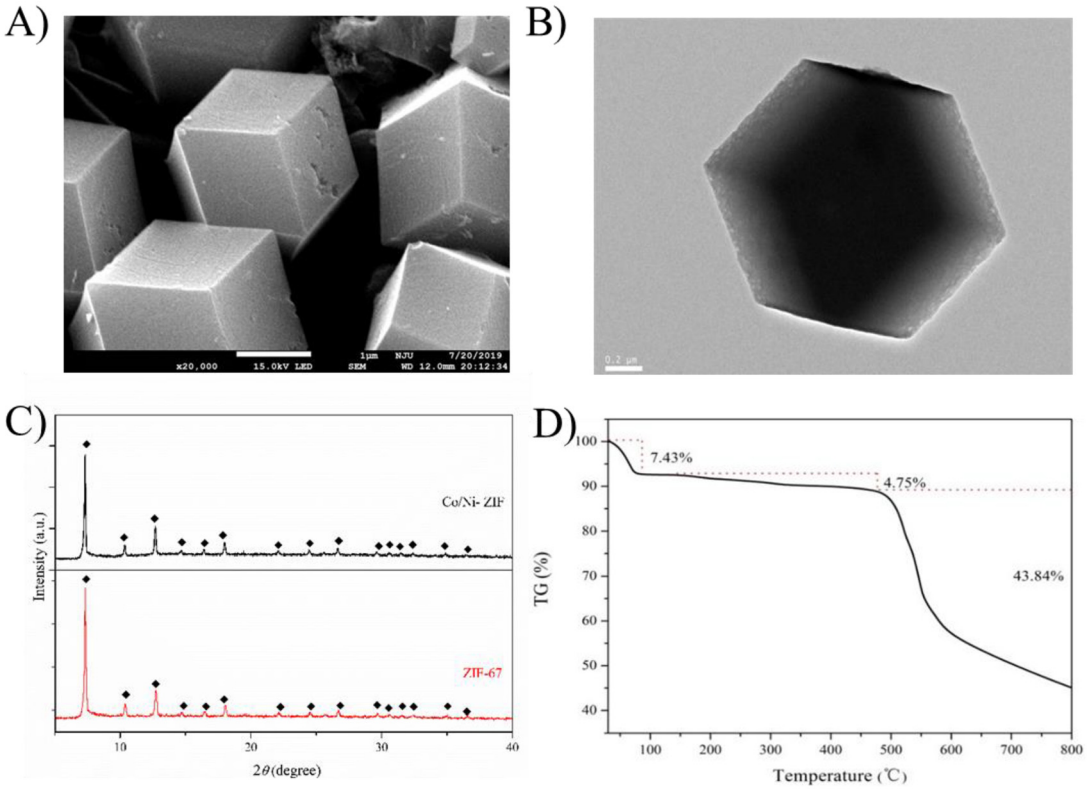

Fig. 1 SEM (A) and TEM (B) images of Co/Ni-ZIF; XRD patterns of ZIF-67 and Co/Ni-ZIF (C); and TGA curve of Co/Ni-ZIF (D). ZIF-67: $Co(NO_3)_2$: $Ni(NO_3)_2$, 5 : 0; Co/Ni-ZIF: $Co(NO_3)_2$: $Ni(NO_3)_2$, 1 : 1.

determined by XRD exhibited similar diffraction patterns with ZIF-67 crystals,[43] indicating that the incorporation of Ni into ZIF-67 at a Co/Ni ratio of 1 : 1 did not alter the topological structure of the crystals (Fig. 1C). Thermogravimetric analysis (TGA) of Co/Ni-ZIF (Fig. 1D) showed three weight-loss steps over a broad temperature range, which could be basically ascribed to the loss of a small number of free guest solvent molecules (such as H_2O and ethanol) in the structure of Co/Ni-ZIF below 100 °C, the loss of high boiling point of excessive 2-MIM from 100 to 500 °C, and the decomposition of the Co/Ni-ZIF frameworks after 500 °C, respectively. Thus, the suitable carbonization temperature of Co/Ni-ZIF precursors is at least above 500 °C. In the present work, 600 °C was chosen as the carbonization temperature. The specific surface area and porous feature of ZIF-67 and Co/Ni-ZIF were further determined by Brunauer–Emmett–Teller (BET) gas-sorption measurements. As shown in Fig. S6A,† ZIF-67 exhibited I type isotherm characteristics similar to microporous materials, while the Co/Ni-ZIF showed a different N_2 sorption isotherm curve referring to micro/mesoporous materials. The BET surface area of ZIF-67 was 1232.92 $m^2\ g^{-1}$, and the corresponding pore-size distribution determined by the Horvath–Kawazoe (HK) method for the microporous region (<2 nm) was about 0.66 nm (inset in Fig. S6A†), verifying the existence of generous micro-pores. After the incorporation of Ni at a Co/Ni ratio of 1 : 1, the BET surface area of the reactant Co/Ni-ZIF decreased to 949.02 $m^2\ g^{-1}$, while the corresponding pore-size distribution determined by the Barrett–Joyner–Halenda (BJH) method for the mesoporous region (2–50 nm) increased to an average diameter of 4 nm, owing to the dissolution of Ni-containing templates in ethanol. Moreover, the single peak with a more narrow size distribution in the Fig. S6B† inset shows that Co/Ni-ZIF possessed a uniform mesopore structure. Thus, the introduction of Ni-containing templates could decrease the specific surface area and increase the micropore diameter of the final Co/Ni-ZIF precursors.

Characterization of Co/Ni-MCN nanocomposites

As shown in Fig. 2A, Co/Ni bimetallic magnetic mesoporous carbon nanocomposites (Co/Ni-MCNs) obtained after carbonization presented a contracted size with an average diameter of 1.0 μm for the rhombic dodecahedra in the SEM image. Furthermore, the TEM image indicated that metal oxides or metals were deposited in carbon matrices of the well dispersed Co/Ni-MCNs without obvious aggregation (Fig. 2B). More detailed information on the porous structure and graphitic degree of Co/Ni-MCNs was obtained from the high-resolution TEM image (Fig. 2C), which clearly showed plentiful mesopores and a rough surface, owing to the carbonization process with the removal of the Ni part from the Co/Ni-ZIF precursors. The interplanar spacing of the crystalline grains was calculated to be 0.28 nm, corresponding to the (220) lattice plane orientation of Co_3O_4.[43] In Fig. 2D, in comparison with the XRD patterns of Co nanoparticles (blue line) and Co_3O_4 nanoparticles

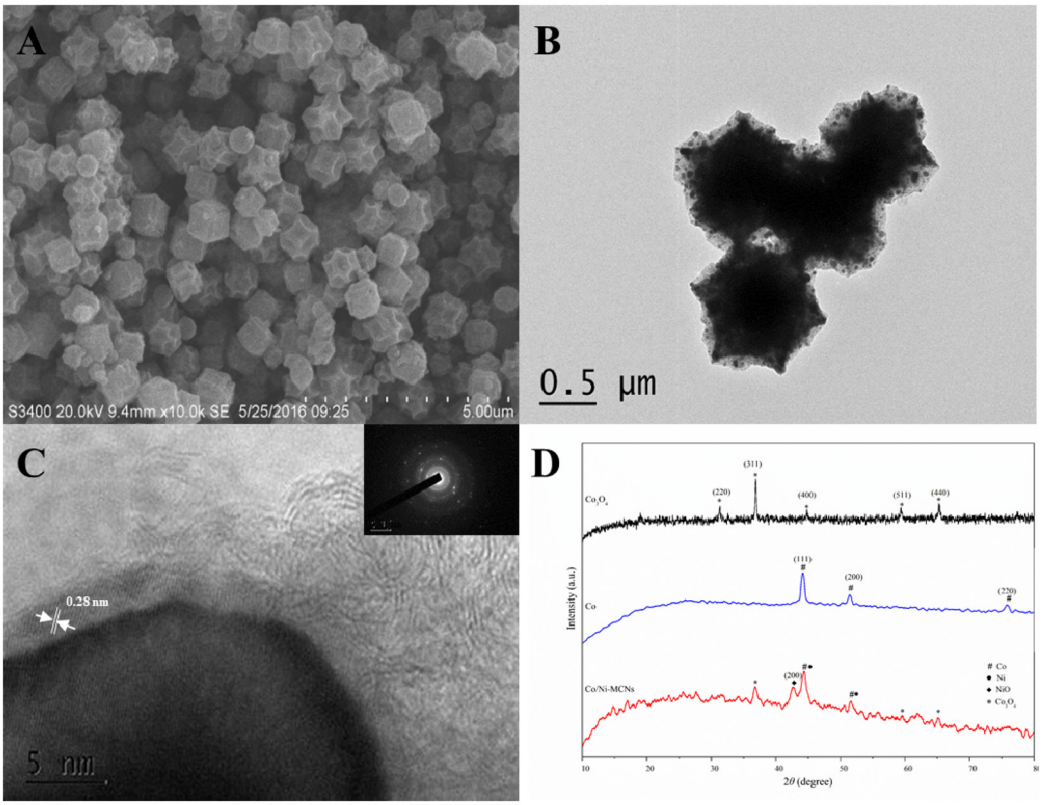

Fig. 2 SEM (A), TEM (B) and HR-TEM images (C) of Co/Ni-MCNs; XRD patterns of Co/Ni-MCNs, as well as Co and Co_3O_4 nanopowders (D).

(black line), the XRD pattern of Co/Ni-MCNs (red line) showed several diffraction peaks, which can be indexed to the (111) and (200) planes of Co fcc crystals (JCPDS no. 15-0806) and the (311), (400), (511) and (440) planes of Co_3O_4 nanoparticles (JCPDS no. 73-1701), respectively. On the other hand, the remaining peaks in the XRD pattern of Co/Ni-MCNs were well indexed to the (111) and (200) planes of Ni fcc crystals (JCPDS card 04-0850) and the (200) plane of NiO nanoparticles (JCPDS no. 17-1049), respectively. All XRD results verified the existence of crystallized Co/Ni nanoparticles in the Co/Ni-MCNs. X-ray photoelectron spectroscopy (XPS) was performed to determine the elemental composition and binding species of carbonized Co/Ni-MCNs (Fig. S7†). The presence of C, N, O, Co and Ni elements was confirmed by the XPS full spectrum. Furthermore, the C 1s peak at around 285 eV could be deconvoluted into three peaks, corresponding to sp^2 hybridized carbon, C–O bonds and C═O/C–N bonds. The high resolution N 1s peak around 400 eV was divided into two peaks corresponding to pyridinic nitrogen and graphitic nitrogen, respectively. The Co 2p spectrum showed a spin coupled doublet for Co 2p3/2 and Co 2p1/2 at 780.1 eV and 796.2 eV, respectively, illustrating the presence of both Co^{2+} and other Co species in Co/Ni-MCNs. Ni 2p3/2 at 855.1 eV and Ni 2p1/2 at 872.5 in the Ni 2p spectrum, respectively, illustrated that Ni^{2+} and Ni existed in the Co/Ni-MCNs. In addition, the FT-IR spectrum of Co/Ni-MCNs (Fig. 3A) indicated that the peaks at 3448 cm^{-1} and 1631 cm^{-1} were attributed to O–H and C═O stretching vibrations, while the peaks at 1422 cm^{-1} and 1384 cm^{-1} in the inset corresponded to C═N and C–N stretching vibrations, respectively. This result confirmed the co-existence of C═O and C–N bonds, which were not distinguished by the deconvolution of the C 1s spectrum in the above XPS measurements. The oxygen- and nitrogen-containing functional groups endowed the Co/Ni-MCNs with good dispersibility in aqueous matrices such as urine and serum. Moreover, it was confirmed that Co/Ni-MCNs were composed of typical graphite shell layers, as well as residual pyridinic nitrogen from 2-MIM and different oxidation states of source metals (Co and Ni) decorated on the carbonized Co/Ni-MCNs. The hysteresis loops (Fig. 3B) illustrated that Co/Ni-MCNs possessed low coercivity with a saturation magnetization (M_s) value of 39.9 emu g^{-1}, being favorable for MSPE due to the excellent magnetic response. The BET surface area and pore diameter of the Co/Ni-MCNs determined by the BJH method were 147.63 m^2 g^{-1} and 3.85 nm, respectively (Fig. 3C and D). The values were lower than those of Co/Ni-ZIF, mainly due to the shrinkage of the material at high temperature for a long time. The Co/Ni-MCN nanocomposites with a large surface area and an enlarged mesopore structure have potential for adsorbing high molecular weight biomolecules such as peptides.

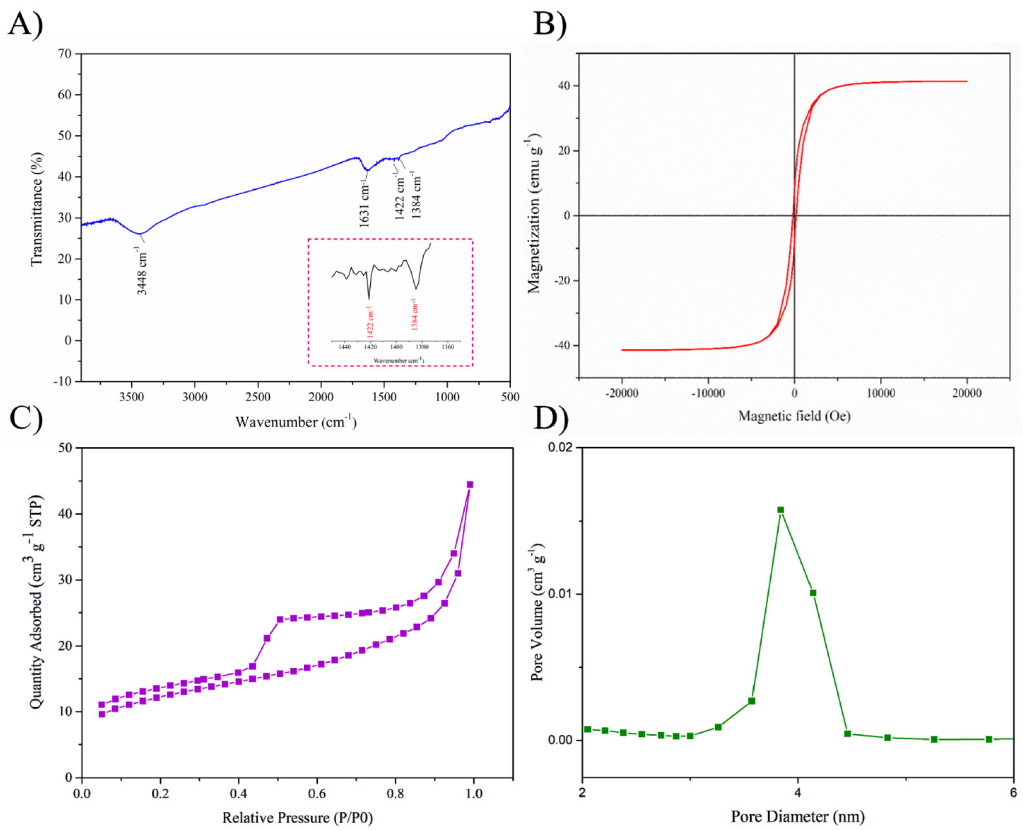

Fig. 3 FT-IR spectrum (A) and magnetic hysteresis loop (B) of Co/Ni-MCNs; N_2 absorption–desorption isotherms of Co/Ni-MCNs (C) and the corresponding pore size distribution (D).

Enrichment performance of Co/Ni-MCNs for endogenous peptides

In order to evaluate the efficiency of the as-prepared Co/Ni-MCNs for enrichment of endogenous peptides, standard angiotensin II was chosen as the model peptide. As shown in Fig. S8,† 5 nM angiotensin II was hardly detected by direct MALDI-TOF MS analysis with a low peak intensity and a signal-to-noise (S/N) ratio of 10.23. After fast MSPE with a Co/Ni-MCN affinity probe, the intensity of angiotensin II increased sharply with an S/N ratio of 1069.49, and the enrichment factor was higher than 100. This high absorbance capacity was attributed to the synergic effects of the hydrophobic interaction of graphitic nitrogen (C–N) and the π–π stacking interaction of pyridinic nitrogen (C═N) toward peptides. In addition, a commercial ZipTipC18 pipette tip was used to enrich the standard peptide for comparison, and the S/N ratio of angiotensin II slightly increased to 91.93 with an enrichment factor of about 10. Therefore, the results illustrated that the Co/Ni-MCN probe possessed high enrichment efficiency for endogenous peptides. To further investigate the enrichment possibility of the Co/Ni-MCNs for low-abundance peptides in more complex matrices, tryptic digests of BSA were employed as the model samples. Fig. 4 shows that only four peptides with weak MS intensity and low S/N ratios were detected in 10 nM BSA digests by MS before enrichment, and ALBU_BOVIN was identified with a low score of 25 and a protein sequence coverage of 5% (MASCOT search results of the ESI†). However, as many as seventeen peptides (score: 126 and sequence coverage: 29%) were trapped by Co/Ni-MCNs, indicating excellent enrichment performance for low-abundance peptides. The detailed information on their amino acid sequences is listed in Table S1.† In contrast, thirteen peptides (score: 39 and sequence coverage: 19%) were detected in the digests after treatment with ZipTipC18.

To assess the sensitivity of the Co/Ni-MCN-based enrichment protocol for low-abundance peptides, different concentrations of BSA tryptic digests were mixed with the affinity probes to capture peptides (Fig. S9†). Three peptides could still be clearly identified even under very low levels of 10 fmol BSA digests, illustrating that the Co/Ni-MCNs have high enrichment sensitivity toward low-abundance peptides. The reusability of the Co/Ni-MCN probes was also tested subsequently. As shown in Fig. S10,† there was no obvious deterioration in the analytical performance after four successive extractions using the same material, indicating that the Co/Ni-MCNs were reusable for peptide enrichment.

Applications of Co/Ni-MCNs for enrichment of endogenous peptides in real biological samples

As common clinical specimens, urine and serum are considered to be very important in disease diagnosis and therapies. Large numbers of analytical methods and technologies have been reported to find biomarkers in human urine and serum. Based on the satisfactory enrichment performance, the as-prepared Co/Ni-MCN nanocomposites were employed for the enrichment of endogenous peptides from human urine samples to examine the feasibility of this affinity probe. In the MALDI-TOF MS spectrum of the diluted urine solution without any pretreatment, no peaks of peptides were observed because of the extremely low concentration in the urine sample. However, after a facile MSPE procedure with Co/Ni-MCNs, as many as twenty-three peaks of peptides were detected with a decent intensity and S/N ratio of MS signals, which demonstrated that the material possessed the ability to enrich low-abundance peptides, while remaining unaffected by the negative influence of urinary and other impurities existing in biological matrices. As a comparison, after solid extrac-

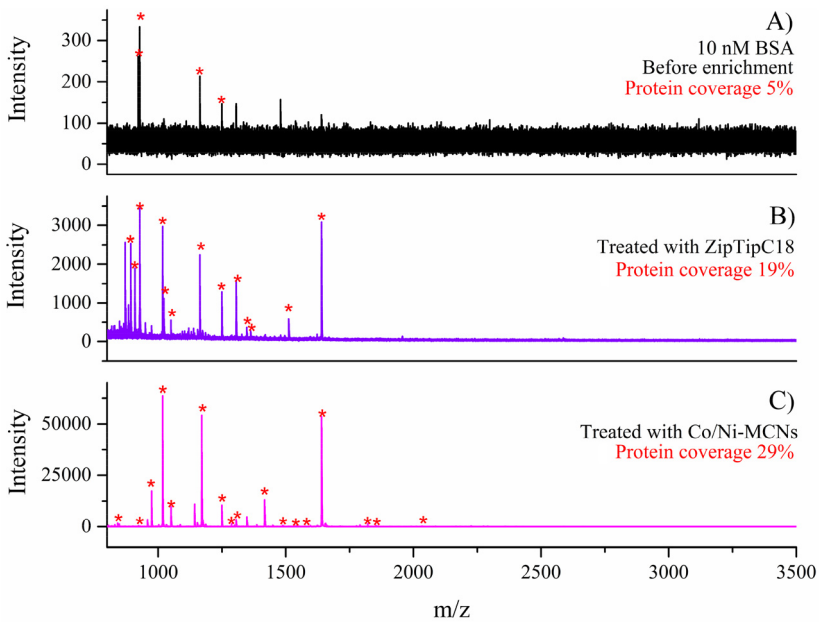

Fig. 4 MS spectra of BSA digests (10 nM) before enrichment (A) and after enrichment with ZiptipC18 (B) and Co/Ni-MCNs (C).

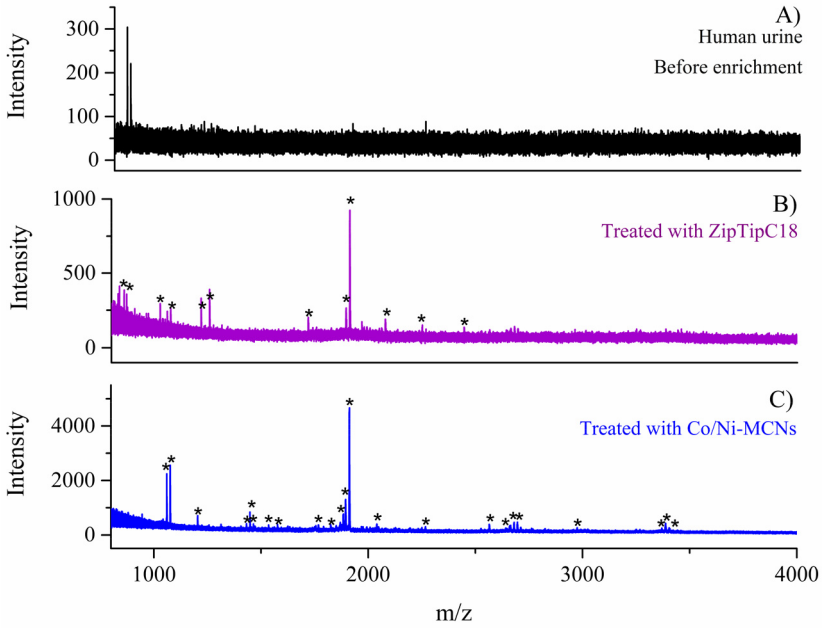

Fig. 5 MS spectra of human urine before enrichment (A) and after enrichment with ZiptipC18 (B) and Co/Ni-MCNs (C).

tion with ZipTipC18, twelve peptides were detected by MS (Fig. 5). We further evaluated the application possibility of the Co/Ni-MCN nanocomposites to enrich endogenous peptides from human serum. Only six peptides were detected in the diluted serum solution before enrichment due to the poor MS signal caused by the low concentration of peptides in the complex matrix. The mass spectrum of the serum profiling with enrichment by Co/Ni-MCNs indicated that sixteen serous peptides were captured and enriched (Fig. S11†). These characteristics confirmed the Co/Ni-MCNs to be a promising affinity probe material in the separation and enrichment of endogenous peptides from real-world complex biological samples.

Comparison with other adsorption materials for low-abundance peptides by magnetic separation

A detailed comparison including the amount of materials taken, enrichment factor toward standard peptides, number of identified peptides from BSA digests, and types of real samples analyzed by the core–shell porous carbon nanocomposites Co/Ni-MCNs, with other magnetic materials, is shown in Table S2.† It can be concluded that the proposed Co/Ni-MCNs prepared using a new and facile preparation in this work have comparable enrichment effects with those magnetic nanomaterials reported in previous works.

Conclusions

In summary, novel mesoporous magnetic Co/Ni-MCN nanocomposites with a rhombic dodecahedron morphology were prepared by using bimetallic ZIFs (Ni-doped ZIF-67) as the precursors. The most interesting aspect of this work is the first-time introduction of nickel and its oxides into Co/Ni-ZIF as sacrificial templates, endowing the Co/Ni-MCNs with a regular framework structure and compatible carbon shells possessing well-defined channels and plentiful mesoporous holes. Subsequently, the developed Co/Ni-MCNs were applied to the MSPE of low-abundance peptides *via* hydrophobic and π–π stacking interactions, followed by MALDI-TOF MS analysis. Due to excellent magnetic properties and reusability, as well as high loading capacity for peptides, Co/Ni-MCNs showed a satisfactory performance in the capture of endogenous peptides in real-world human urine and serum samples. This sacrificial template method using MOFs as precursors is also expected to facilitate the development of new solid-phase extraction materials to efficiently separate and enrich other types of biological analytes in future peptidomic/proteomic studies.

Ethical statement

Human serum and urine samples were provided by healthy volunteers and approved by the Medical Ethical Committee of the First Affiliated Hospital of Nanjing Medical University.

Author contributions

Jia-Yuan Li: investigation, methodology, formal analysis, data curation, visualization and writing – original draft. Sen Zhang: investigation, formal analysis, data curation and visualization. Wan-Yue Zhuang: methodology, data curation and visualization. Feng Zhang: formal analysis and visualization. Wei-Juan Zheng: methodology and resources. Hong-Zhen Lian: conceptualization, resources, project administration, supervision, funding acquisition and writing – review & editing.

Data availability

The data supporting this article have been included as part of the ESI.†

Conflicts of interest

There are no conflicts to declare.

Acknowledgements

This work was supported by the National Key R&D Program of China (no. 2024YFF0618100) and the National Natural Science Foundation of China (22176085 and 21874065).

References

1 L. A. Liotta and E. F. Petricoin, *J. Clin. Invest.*, 2006, **116**, 26–30.
2 E. F. Petricoin, C. Belluco, R. P. Araujo and L. A. Liotta, *Nat. Rev. Cancer*, 2006, **6**, 961–967.
3 A. Abbott, *Nature*, 2001, **409**, 747–748.
4 Y. Oda, T. Nagasu and B. T. Chait, *Nat. Biotechnol.*, 2001, **19**, 379–382.
5 H. Q. Qin, P. Gao, F. J. Wang, L. Zhao, J. Zhu, A. Q. Wang, T. Zhang, R. A. Wu and H. F. Zou, *Angew. Chem., Int. Ed.*, 2011, **50**, 12218–12221.
6 Z. Y. Gu, Y. J. Chen, J. Q. Jiang and X. P. Yan, *Chem. Commun.*, 2011, **47**, 4787–4789.
7 Y. H. Zhang, X. Y. Wang, W. Shan, B. Y. Wu, H. Z. Fan, X. J. Yu, Y. Tang and P. Y. Yang, *Angew. Chem., Int. Ed.*, 2005, **44**, 615–617.
8 X. Li, S. Y. Xu, C. S. Pan, H. J. Zhou, X. G. Jiang, Y. Zhang, M. L. Ye and H. F. Zou, *J. Sep. Sci.*, 2007, **30**, 930–943.
9 N. S. Ye, *Anal. Lett.*, 2008, **41**, 2554–2563.
10 M. Jiang, L. Y. Qi, P. R. Liu, Z. J. Wang, Z. G. Duan, Y. Wang, Z. H. Liu and P. Chen, *J. Chromatogr. B*, 2016, **1027**, 149–157.
11 R. J. Tian, H. Zhang, M. L. Ye, X. G. Jiang, L. H. Hu, X. Li, X. H. Bao and H. F. Zou, *Angew. Chem., Int. Ed.*, 2007, **46**, 962–965.
12 H. M. Xiong, X. Y. Guan, L. H. Jin, W. W. Shen, H. J. Lu and Y. Y. Xia, *Angew. Chem., Int. Ed.*, 2008, **47**, 4204–4207.
13 W. T. Jia, X. H. Chen, H. J. Lu and P. Y. Yang, *Angew. Chem., Int. Ed.*, 2006, **45**, 3345–3349.
14 W. W. Shen, H. M. Xiong, Y. Xu, S. J. Cai, H. J. Lu and P. Y. Yang, *Anal. Chem.*, 2008, **80**, 6758–6763.
15 Z. C. Xiong, Y. S. Ji, C. L. Fang, Q. Q. Zhang, L. Y. Zhang, M. L. Ye, W. B. Zhang and H. F. Zou, *Chem. – Eur. J.*, 2014, **20**, 7389–7395.
16 M. Zhao, C. H. Deng, X. M. Zhang and P. Y. Yang, *Proteomics*, 2013, **13**, 3387–3392.
17 M. Zhao, Y. Q. Xie, H. M. Chen and C. H. Deng, *Talanta*, 2017, **167**, 392–397.
18 Q. Liu, J. B. Shi, M. T. Cheng, G. L. Li, D. Cao and G. B. Jiang, *Chem. Commun.*, 2012, **48**, 1874–1876.
19 P. Yin, N. R. Sun, C. H. Deng, Y. Li, X. M. Zhang and P. Y. Yang, *Proteomics*, 2013, **13**, 2243–2250.
20 H. M. Chen, S. S. Liu, H. L. Yang, Y. Mao, C. H. Deng, X. M. Zhang and P. Y. Yang, *Proteomics*, 2010, **10**, 930–939.
21 G. T. Zhu, X. S. Li, Q. Gao, N. W. Zhao, B. F. Yuan and Y. Q. Feng, *J. Chromatogr. A*, 2012, **1224**, 11–18.
22 Q. Song, W. J. Zhao, H. X. Yin and H. Z. Lian, *RSC Adv.*, 2015, **5**, 63896–63902.
23 X. Y. Long, Z. J. Zhang, J. Y. Li, D. Sheng and H. Z. Lian, *Anal. Chem.*, 2017, **89**, 10446–10453.
24 H. Wan, H. Q. Qin, Z. C. Xiong, W. B. Zhang and H. F. Zou, *Nanoscale*, 2013, **5**, 10936–10944.
25 L. L. Sun, Q. Zhao, G. J. Zhu, Y. Zhou, T. T. Wang, Y. C. Shan, K. G. Yang, Z. Liang, L. H. Zhang and Y. K. Zhang, *Rapid Commun. Mass Spectrom.*, 2011, **25**, 1257–1265.
26 H. M. Chen, C. H. Deng, Y. Li, Y. Dai, P. Y. Yang and X. M. Zhang, *Adv. Mater.*, 2009, **21**, 2200–2205.
27 H. M. Chen, X. Q. Xu, N. Yao, C. H. Deng, P. Y. Yang and X. M. Zhang, *Proteomics*, 2008, **8**, 2778–2784.
28 M. Zhao, C. H. Deng and X. M. Zhang, *ChemPlusChem*, 2014, **79**, 359–365.
29 H. M. Chen, C. H. Deng and X. M. Zhang, *Angew. Chem., Int. Ed.*, 2010, **49**, 607–611.
30 H. M. Chen, D. W. Qi, C. H. Deng, P. Y. Yang and X. M. Zhang, *Proteomics*, 2009, **9**, 380–387.
31 Y. Q. Zhao, H. B. Li, H. J. Zheng and Q. Jia, *Anal. Chem.*, 2025, **97**, 1135–1142.
32 B. F. Zhao, W. H. Xu, J. T. Ma and Q. Jia, *Chin. Chem. Lett.*, 2023, **34**, 107498.
33 H. L. Huang, J. R. Li, K. K. Wang, T. T. Han, M. M. Tong, L. S. Li, Y. B. Xie, Q. Y. Yang, D. H. Liu and C. L. Zhong, *Nat. Commun.*, 2015, **6**, 8847.
34 Z. Q. Sun, B. W. Sun, J. J. Xue, J. H. He, R. Z. Zhao, Z. H. Chen, Z. X. Sun, H. K. Liu and S. X. Dou, *Adv. Funct. Mater.*, 2025, **35**, 2414671.
35 G. H. Zhong, D. X. Liu and J. Y. Zhang, *J. Mater. Chem. A*, 2018, **6**, 1887–1899.
36 S. Saghir, S. J. Zhang, Y. Q. Wang, E. F. Fu, Z. G. Xiao, A. H. Zahid and C. K. Pu, *J. Environ. Chem. Eng.*, 2024, **12**, 113166.
37 H. S. Jadhav, H. A. Bandal, S. Ramakrishna and H. Kim, *Adv. Mater.*, 2022, **34**, 2107072.
38 V. R. Bheeram, A. S. Dadhich and S. B. Mukkamala, *Inorg. Chem. Commun.*, 2023, **150**, 110455.
39 M. Hu, J. Reboul, S. Furukawa, N. L. Torad, Q. M. Ji, P. Srinivasu, K. Ariga, S. Kitagawa and Y. Yamauchi, *J. Am. Chem. Soc.*, 2012, **134**, 2864–2867.
40 L. Zhang, H. B. Wu, S. Madhavi, H. H. Hng and X. W. Lou, *J. Am. Chem. Soc.*, 2012, **134**, 17388–17391.

41 F. C. Zheng, D. Q. Zhu, X. H. Shi and Q. W. Chen, *J. Mater. Chem. A*, 2015, **3**, 2815–2824.
42 A. Banerjee, R. Gokhale, S. Bhatnagar, J. Jog, M. Bhardwaj, B. Lefez, B. Hannoyer and S. Ogale, *J. Mater. Chem.*, 2012, **22**, 19694–19699.
43 R. B. Wu, X. K. Qian, X. H. Rui, H. Liu, B. Yadian, K. Zhou, J. Wei, Q. Y. Yan, X. Q. Feng, Y. Long, L. Y. Wang and Y. Z. Huang, *Small*, 2014, **10**, 1932–1938.
44 N. L. Torad, M. Hu, S. Ishihara, H. Sukegawa, A. A. Belik, M. Imura, K. Ariga, Y. Sakka and Y. Yamauchi, *Small*, 2014, **10**, 2096–2107.
45 S. Thimmarayan, H. Mohan, B. M. K. Vasamsetti, G. Kim, K. Natesan, A. Jayaprakash and T. Shin, *Chemosphere*, 2024, **347**, 140680.
46 J. F. Qian, F. A. Sun and L. Z. Qin, *Mater. Lett.*, 2012, **82**, 220–223.
47 C. X. Duan, Y. Yu and H. Hu, *Green Energy Environ.*, 2022, **7**, 3–15.
48 J. Y. Li, X. Y. Long, D. Sheng and H. Z. Lian, *Talanta*, 2020, **208**, 120437.
49 W. Z. Xu, X. L. Wang, Y. Wu, W. Li and C. Y. Chen, *J. Hazard. Mater.*, 2019, **363**, 138–151.